International Journal of Earth, Energy and Environmental Sciences
ISSN: 2517-942X
Vol:5, No:3, 2011

Discontinuous Galerkin Method for 1D Shallow Water Flow with Water Surface Slope Limiter

W. Lai and A. A. Khan

***Abstract*—**A water surface slope limiting scheme is tested and compared with the water depth slope limiter for the solution of one dimensional shallow water equations with bottom slope source term. Numerical schemes based on the total variation diminishing Runge-Kutta discontinuous Galerkin finite element method with slope limiter schemes based on water surface slope and water depth are used to solve one-dimensional shallow water equations. For each slope limiter, three different Riemann solvers based on HLL, LF, and Roe flux functions are used. The proposed water surface based slope limiter scheme is easy to implement and shows better conservation property compared to the slope limiter based on water depth. Of the three flux functions, the Roe approximation provides the best results while the LF function proves to be least suitable when used with either slope limiter scheme.

***Keywords*—**Discontinuous finite element, TVD Runge-Kutta scheme, slope limiters, Riemann solvers, shallow water flow.

I. Introduction

OPEN channel flow problems are governed by the shallow water equations (SWE), also known as Saint-Venant equations. Over the past decades, several numerical schemes have been developed to solve the shallow water equations for various applications. The finite difference method (FDM) and finite volume method (FVM) are the two most widely used methods for shallow water equations and fluid dynamics problems. Wang et al. [1] used a finite difference TVD scheme to compute dam break problem. Lin et al. [2] used finite volume method to solve shallow water equations.

In general, finite element method (FEM) is preferred for complex geometries. However, traditional finite element method fails to model the convective terms in general fluid dynamics problems and extra efforts are required to overcome this shortcoming, such as penalty finite element method [3], split-characteristic finite element method [4], characteristic-mixed finite element method [5] and so on.

In recent years, the discontinuous Galerkin (DG) method has been developed to solve systems of hyperbolic equations. The DG method was first introduced by Reed and Hill [6] for the solution of neutron transport equation, a time independent linear hyperbolic equation. Cockburn and Shu [7], Cockburn et al. [8], Cockburn et al. [9], and Cockburn et al. [10] further advanced the DG method for conservation laws and incorporated TVD explicit Runge-Kutta time integration scheme along with flux limiters or slope limiters to ensure the TVD properties for discontinuous Galerkin method. The Runge-Kutta discontinuous Galerkin (RKDG) method can be viewed as a combination of finite volume method and finite element method. As a result, the RKDG method keeps advantages of both FVM and FEM. As discontinuous elements are used, various upwind scheme used in FVM may be incorporated into RKDG method to deal with convective dominated problems. Like the FEM, RKDG method can deal with complex geometry conveniently and can utilize higher order spatial approximation. According to Li [11], the RKDG method provides additional advantages. For example, RKDG method can easily deal with source term as in FEM. By decoupling the elements through the use of boundary flux, a local formulation is achieved that does not require assembling the global matrix and explicit time schemes can be locally applied at an element level. In practical applications, where millions of elements may be used, the RKDG method will prove advantageous in terms computing speed and memory demand. The RKDG method is a conservative scheme, which is a suitable choice for physical problems, since most physical properties such as mass and momentum are conservative. As the solution of DG method is discontinuous, it can be easily adopted for problems involving shocks and discontinuities. In addition, the hp-adaptive algorithm is much easier to apply to the RKDG local formulation.

Schwanebberg and Köngeter [12] were the first to implement the RKDG method for shallow water equations for applications to practical problems like shocks, dam-break problem, and oblique hydraulic jump. Later Schwanenberg and Harms [13] used different cases in transcritical flow to investigate the accuracy and convergence of RKDG method. Aizinger and Dawson [14] and Dawson and Aizinger [15] applied the RKDG method to two-dimensional and three-dimensional shallow water flows. Kubatko et al. [16] demonstrated the applicability of hp-adaptive algorithm for RKDG method.

In the DG method, the elements are decoupled and the accuracy with which the boundary flux is calculated determines the performance of the method. The calculation of boundary flux becomes a generalized Riemann problem (GRP). Since the exact Riemann solvers are tedious and time-consuming, different approximate Riemann solvers are developed in recent decades, such as HLL flux [17] and Roe flux [18]. Schwanenberg and Harms [13] used RKDG method with HLL flux to test one and two dimensional dam break problems, while Tassi et al. [19] incorporated HLLC flux for shallow water flow problems.

As in other numerical schemes, using higher order spatial

W. Lai is with the Department of Civil Engineering, Clemson University, Clemson, SC 29634, USA (e-mail: wlai@clemson.edu).

A. A. Khan is with the Department of Civil Engineering, Clemson University, Clemson, SC 29634, USA (e-mail: abdkha@clemson.edu).

approximation in RKDG method results in unphysical spurious oscillation. To circumvent the problem, the scheme must satisfy the Total Variation Diminishing (TVD) criterion. Flux limiters and slope limiters are widely used to achieve the TVD property. Gottlieb and Shu [20] showed that a TVD spatial discretization may generate oscillation with non-TVD Runge-Kutta time discretization. Cockburn and Shu [7] demonstrated that for piecewise polynomials of r^{th} order, with a $(r+1)^{th}$ order TVD time integration, the results were $(r+1)^{th}$ order accurate. They further proved that the scheme was total variation bounded in the means (TVBM), which is a modification of the TVD property.

In addition to the difficulty of dealing with convective terms in traditional methods, problems arise when the source term appear. Zhou et al. [21] developed the surface gradient method to treat the source term in the shallow water equation for the data reconstruction. Ying et al. [22] devised a weighted average water surface gradient approach to deal with source term in one dimensional open channel flows, the weighted factors were based on the Courant number. Catella et al. [23] proposed a predictor-corrector finite volume method to compute one-dimensional open channel flows. The proposed method did not need to solve the Riemann problem at cell interface and artificial viscosity or shock-capturing techniques were not needed to capture discontinuities. A Froude number based criterion was used to overcome the difficulty of handling the source term.

In this paper, Runge-Kutta discontinuous Galerkin method with TVD based water surface slope limiting scheme for the source term is proposed for solving one-dimensional shallow water equations. The TVD based slope limiter scheme is usually applied to the conservative variables of the hyperbolic system to preserve the conservative property of the system. Here, the water surface based slope limiter is applied and the numerical results are compared to the slope limiter based on the water depth. Three different flux functions are investigated for each slope limiter scheme. Two channels with variable bed slopes are used to test the scheme with different flow conditions. The numerical results show a better conservation property with the water surface based slope limiter scheme.

II. Formulation of Discontinuous Galerkin Method

The conservative form of one-dimensional shallow water flow equations for a rectangular channel, as given by the Saint-Venant equations, is given by

$$\frac{\partial \mathbf{U}}{\partial t}+\frac{\partial \mathbf{F}}{\partial x}=\mathbf{S} \tag{1}$$

where **U** is the conservative variable vector, **F** is the flux vector, and **S** is the source vector. These terms can be expressed as

$$\mathbf{U}=\begin{bmatrix} h \\ q \end{bmatrix}, \mathbf{F}=\begin{bmatrix} q \\ gh^2/2+q^2/h \end{bmatrix}, \mathbf{S}=\begin{bmatrix} 0 \\ gh\left(S_o-S_f\right) \end{bmatrix} \tag{2}$$

where S_o is the bed slope, S_f is the energy slope as given by Manning's equation, h is the depth of flow, and q is the discharge per unit width. The Jacobian matrix for the shallow water equation is

$$\mathbf{A}=\frac{\partial \mathbf{F}}{\partial \mathbf{U}}=\begin{bmatrix} 0 & 1 \\ gh-q^2/h^2 & 2q/h \end{bmatrix}. \tag{3}$$

The eigen values of the Jacobian matrix are

$$\lambda_1=q/h-\sqrt{gh}=u-c,\ \lambda_2=q/h+\sqrt{gh}=u+c \tag{4}$$

and the two independent eigen vectors are

$$\mathbf{K}_1=\left[1,u-c\right]^T,\quad \mathbf{K}_2=\left[1,u+c\right]^T. \tag{5}$$

Applying the discontinuous Galerkin method to the continuity and momentum equations over an element (x_1, x_2) gives

$$\begin{aligned}&\int_{x_1}^{x_2} N_i dx\frac{\partial \hat{h}}{\partial t}-\int_{x_1}^{x_2}\frac{\partial N_i}{\partial x}\hat{q}dx+\\&N_i\left(x_2\right)P(x_2,t)-N_i\left(x_1\right)P(x_1,t)=0\end{aligned} \tag{6}$$

$$\begin{aligned}&\int_{x_1}^{x_2} N_i dx\frac{\partial \hat{q}}{\partial t}-\int_{x_1}^{x_2}\frac{\partial N_i}{\partial x}\left(\hat{q}^2/\hat{h}+g\hat{h}^2/2\right)dx\\&+N_i\left(x_2\right)G(x_2,t)-N_i\left(x_1\right)G(x_1,t)=\\&\int_{x_1}^{x_2} N_i\left(g\hat{h}\hat{S}_o-g\hat{h}\hat{S}_f\right)dx\end{aligned} \tag{7}$$

where $P(x,t)=q$ is the flux function for the continuity equation and $G(x,t)=q^2/h+gh^2/2$ is the flux function for the momentum equation. These flux function at the element boundaries are calculated using approximate Riemann solvers. The approximate variables $\hat{h}$ and $\hat{q}$ as well as any function $\hat{f}(h,q)$ can be expressed as

$$\hat{h}=N_j h_j,\ \hat{q}=N_j q_j,\ \hat{f}(h,q,n)=f(\hat{h},\hat{q},\hat{n}) \tag{8}$$

where N_i, N_j represent test and shape functions and h_j, q_j, etc. represent discrete values.

III. Numerical Flux functions

Since a discontinuity is allowed across the element interface, the numerical flux normal to the element interface can be attained from the local Riemann solver given the left and right states. Since the exact Riemann solvers are complex and time consuming, various approximate Riemann solvers

are available to give fast approximate solutions to the problem. The flux functions used are described below.

A. HLL Flux

$$\mathbf{F}^{HLL}\left(\mathbf{U}^{-},\mathbf{U}^{+}\right)=\begin{cases}\mathbf{F}^{-}, & 0\le S_L\\ \dfrac{S_R\mathbf{F}^{-}-S_L\mathbf{F}^{+}+S_LS_R\left(\mathbf{U}^{+}-\mathbf{U}^{-}\right)}{S_R-S_L}, & S_L\le 0\le S_R\\ \mathbf{F}^{+}, & 0\ge S_R\end{cases} \tag{9}$$

$$\begin{aligned}S_L&=\min\left(u^{-}-\sqrt{gh^{-}},u^{+}-\sqrt{gh^{+}}\right),\\ S_R&=\max\left(u^{-}+\sqrt{gh^{-}},u^{+}+\sqrt{gh^{+}}\right)\end{aligned} \tag{10}$$

where $\mathbf{F}^{-}=\mathbf{F}(\mathbf{U}^{-})$ and $\mathbf{F}^{+}=\mathbf{F}(\mathbf{U}^{+})$. In general, f^{+} represents the value of f just downstream of a node (from the downstream element) and f^{-} is the value of f just upstream of a node (from upstream element).

B. Lax-Friedrichs Flux

The wave speed in this case, for $S_L=-S^{+}$ and $S_R=S^{+}$, is estimated as

$$S^{+}=\max\left(\left|u^{-}\right|+\sqrt{gh^{-}},\left|u^{+}\right|+\sqrt{gh^{+}}\right) \tag{11}$$

and the LF flux is given as

$$\mathbf{F}^{LF}=\frac{1}{2}\left(\mathbf{F}^{-}+\mathbf{F}^{+}\right)-\frac{1}{2}S^{+}\left(\mathbf{U}^{+}-\mathbf{U}^{-}\right). \tag{12}$$

C. Roe Flux

$$\mathbf{F}^{Roe}=\frac{1}{2}\left(\mathbf{F}^{-}+\mathbf{F}^{+}\right)-\frac{1}{2}\sum_{i=1}^{2}\tilde{\alpha}_i\left|\tilde{\lambda}_i\right|\tilde{\mathbf{K}}_i \tag{13}$$

$$\tilde{\alpha}_1=\frac{1}{2}\left(\Delta h-\frac{\tilde{h}\Delta u}{\tilde{c}}\right),\ \tilde{\alpha}_2=\frac{1}{2}\left(\Delta h+\frac{\tilde{h}\Delta u}{\tilde{c}}\right) \tag{14}$$

$$\Delta h=h^{+}-h^{-},\ \Delta u=u^{+}-u^{-},\ \tilde{c}=\sqrt{\frac{g\left(h^{-}+h^{+}\right)}{2}} \tag{15}$$

$$\tilde{h}=\sqrt{h^{-}h^{+}},\ \tilde{u}=\frac{\sqrt{h^{-}}u^{-}+\sqrt{h^{+}}u^{+}}{\sqrt{h^{-}}+\sqrt{h^{+}}} \tag{16}$$

The eigen values $\tilde{\lambda}$ and the eigen vectors $\tilde{\mathbf{K}}$ are calculated using the new variables.

IV. Runge-Kutta TVD Time Integration

The TVD Runge-Kutta time scheme should be one order higher than the order of the spatial or shape functions [7], [8], [9]. Equations (6) and (7) can be written as

$$\frac{\partial\mathbf{U}}{\partial t}=L\left(\mathbf{U}\right) \tag{17}$$

and for linear shape functions within an element, the TVD second order Runge-Kutta scheme [20] is given by

$$\begin{aligned}\mathbf{U}^{[1]}&=\mathbf{U}^{n}+\Delta tL\left(\mathbf{U}^{n}\right),\\ \mathbf{U}^{n+1}&=\frac{1}{2}\mathbf{U}^{n}+\frac{1}{2}\mathbf{U}^{[1]}+\frac{1}{2}\Delta tL\left(\mathbf{U}^{[1]}\right)\end{aligned} \tag{18}$$

with the explicit scheme, the Courant-Friedrichs-Lewy (CFL) condition is required for the stability. The CFL condition is given by

$$\max\left[\frac{\Delta t}{\Delta x}\left(\left|u\right|+c\right)\right]_{\forall\text{elements}}\le\frac{1}{2r+1} \tag{19}$$

where *r* is the order of polynomials for space discretization [24].

V. Water Surface Slope Limiting

A slope limiter is used to eliminate an oscillatory solution at a sharp front. Originally the slope limiter is applied to the conservative variables to maintain the conservation property of the system. However, in shallow water flow with bed slope, the Saint-Venant equations give numerically generated flow even for zero water surface gradient. To overcome this drawback, the slope limiter based on the water surface elevation instead of the water depth may be applied. For an element *l*, the water surface slope limiter is given by

$$\tilde{Z}(x)=\overline{Z}(x)+(x-x_{l,mid})\sigma_l,\quad x_1\le x\le x_2 \tag{20}$$

and for bed elevation z_b, the average water surface elevation, $\overline{Z}(x)$, over an element is given by

$$\overline{Z}(x)=\frac{1}{(x_2-x_1)}\int_{x_1}^{x_2}Z\,dx\quad\text{and}\quad Z=z_b+h. \tag{21}$$

Here the monotonized central slope limiter is used and is given by

$$\sigma_l=sign(a,b)\min\left(\frac{|a+b|}{2},2|a|,2|b|\right) \tag{22}$$

where the upwind slope *a* and downwind slope *b* are given by

$$a = \frac{\overline{Z}_l - \overline{Z}_{l-1}}{(x_{l,mid} - x_{l-1,mid})}, b = \frac{\overline{Z}_{l+1} - \overline{Z}_l}{(x_{l+1,mid} - x_{l,mid})} \quad (23)$$

and $x_{l,mid}$ is the *x* value at the midpoint of the element.

VI. Numerical Tests

A. Test 1

A frictionless 1 *m* wide 25 *m* long rectangular channel with a bump was used for this test. The initial water level was fixed at 0.33 *m* and the flows in and out of the channel were set to zero. The bed elevation was given by

$$z_b = \begin{cases} 0.2 - 0.05(x-10)^2 & 8 \le x \le 12 \\ 0 \quad \text{otherwise} \end{cases} \quad (24)$$

and described a bump in the bed.

Simulation results of water surface elevation and discharge per unit width for the three different flux functions, with slope limiters based on water depth and water surface, are shown in Figs. 1 to 4. Numerical results show that when the slope limiter based on the water depth slope is used, there are small oscillations in water depth and there is unphysical flow rate of the order of 0.001 m^2/s. On the other hand, when the slope limiter based on the water surface slope is used, there is no water surface oscillation, and the flow rate drops to the order of 10^{-7} m^2/s. In addition, for each of the slope limiter, the three different flux functions give results of the same order of accuracy.

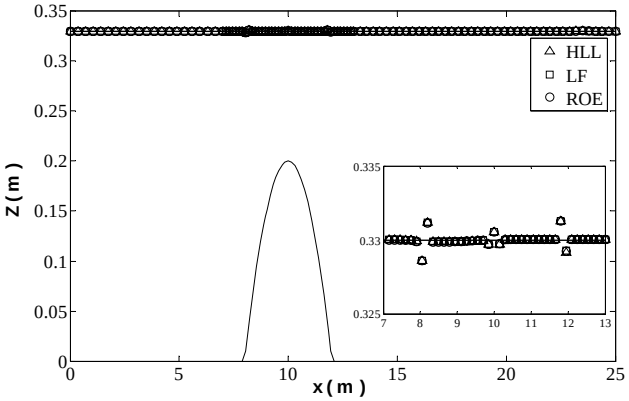

Fig. 1 Numerical solution of water depth for Test 1 with water depth slope limiter

B. Test 2

For this test, the channel width, length, and bed elevation were as described for Test 1. In this case, the flow rate at the inflow boundary was set to 0.18 m^2/s and the downstream water surface elevation was set to 0.5 m, describing a subcritical flow condition in the channel.

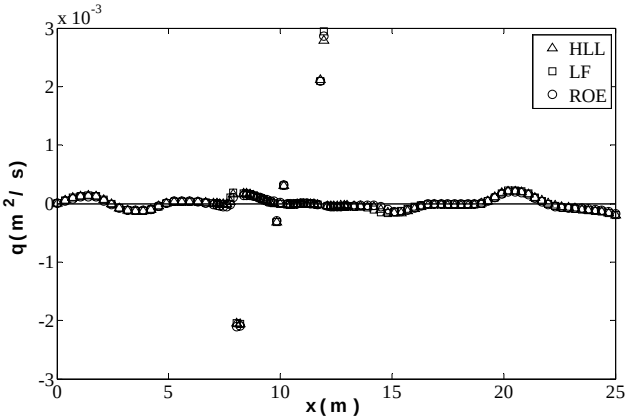

Fig. 2 Numerical solution of flow rate for Test 1 with water depth slope limiter

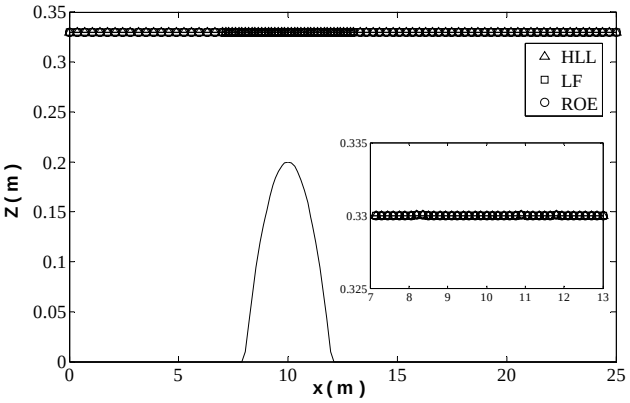

Fig. 3 Numerical solution of water depth for Test 1 with water surface slope limiter

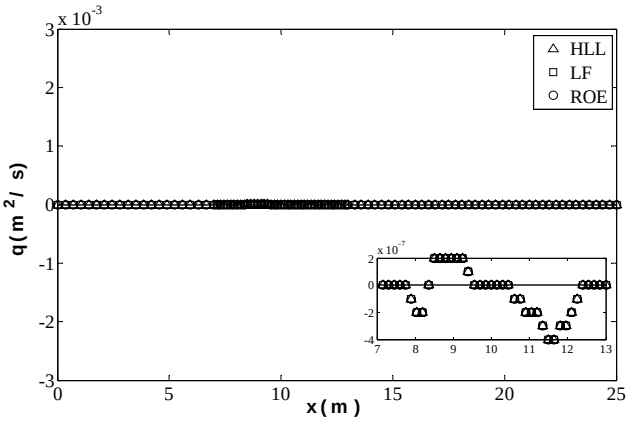

Fig. 4 Numerical solution of flow rate for Test 1 with water surface slope limiter

The results of water surface and flow rate for the two slope limiters with three different flux approximations in each case are given in Figs 5 to 8. The water surface result shows oscillatory solution at the beginning and end of the bump for all three flux functions with water depth slope limiter. Whereas the water surface is predicted accurately using the water surface slope limiter. The result for flow rate in case of

water depth slope limiter shows large oscillations over the bump. However, the water surface slope limiter preserves the conservation property.

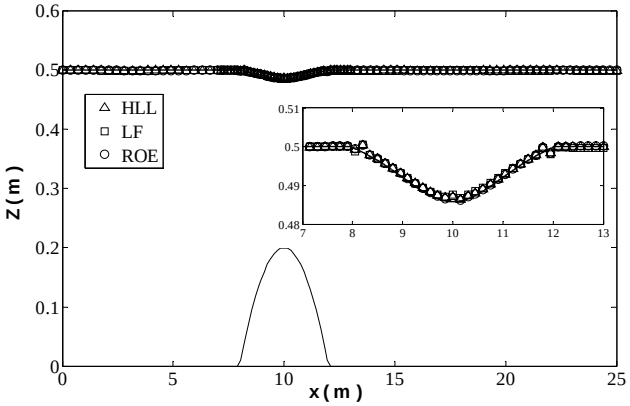

Fig. 5 Numerical solution of water depth for Test 2 with water depth slope limiter

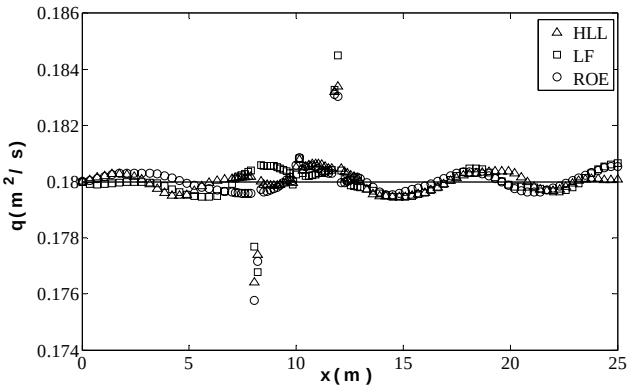

Fig. 6 Numerical solution of flow rate for Test 2 with water depth slope limiter

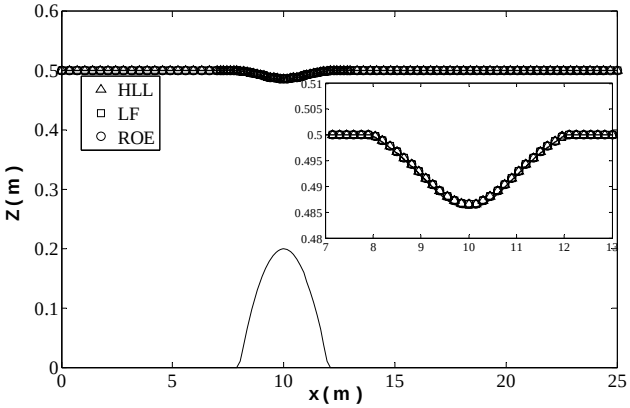

Fig. 7 Numerical solution of water depth for Test 2 with water surface slope limiter

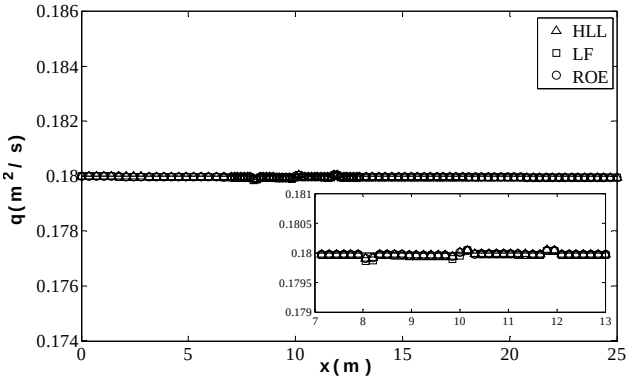

Fig. 8 Numerical solution of flow rate for Test 2 with water surface slope limiter

C. Test 3

The channel width, length, and bed topography were as described for the previous two tests. Inflow boundary condition was set to 0.18 m^2/s and downstream water surface elevation was fixed at 0.33 *m*. The flow regime changed from subcritical to supercritical and back to subcritical flow through a hydraulic jump.

The numerical results for this test are shown in Figs. 9 to 12. In the figures, the solid line shows the analytical result. The water surface level is predicted accurately by both slope limiters using three different flux functions. As before the simulation results of water surface based slope limiter provide better conservation properties for discharge than the water depth based slope limiter. Of the three flux functions, Roe flux conserves the flow rate most accurately and when used with case water surface based flow limiter the discharge is constant throughout the domain.

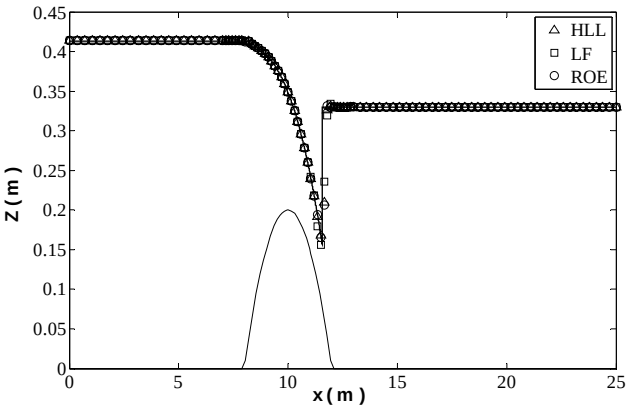

Fig. 9 Numerical solution of water depth for Test 3 with water depth slope limiter

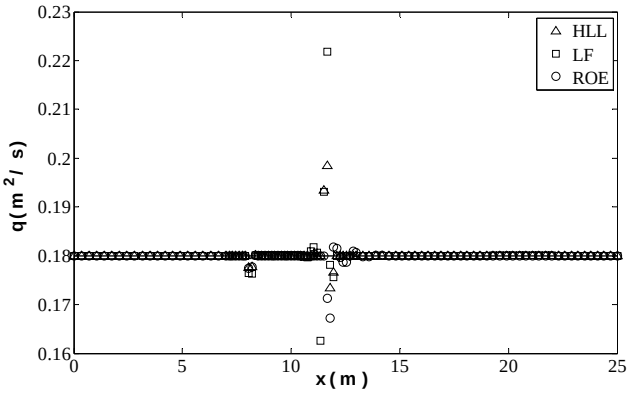

Fig. 10 Numerical solution of flow rate for Test 3 with water depth slope limiter

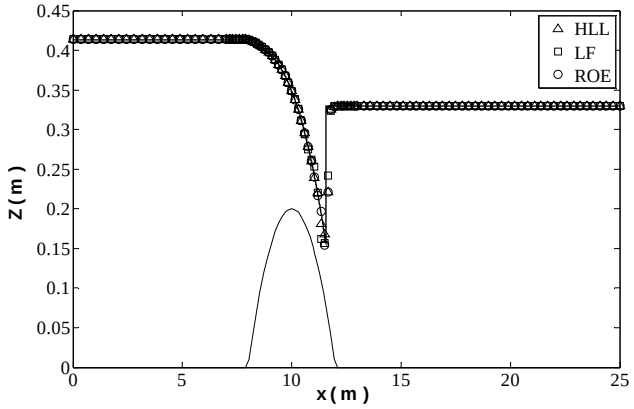

Fig. 11 Numerical solution of water depth for Test 3 with water surface slope limiter

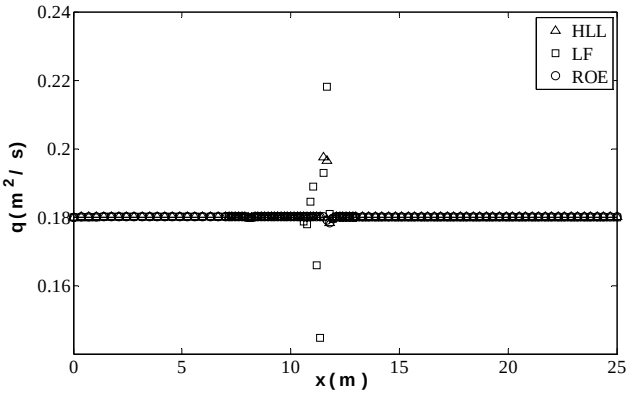

Fig. 12 Numerical solution of flow rate for Test 3 with water surface slope limiter

D.Test 4

For the channel geometry and bed topography as described for the previous test cases, the inflow discharge per unit width and flow depth at the upstream end was set to 25.0567 m^2/s and 2 *m*, respectively. The flow is supercritical throughout the domain.

The simulation results of water surface and discharge are shown in Figs. 13 to 16. For this supercritical flow test, the simulation results of water depth and flow rate have the same accuracy when the HLL and Roe flux functions are used with water surface or water depth slope limiters. However for both slope limiters, the LF flux function gives unphysical oscillations for flow rate.

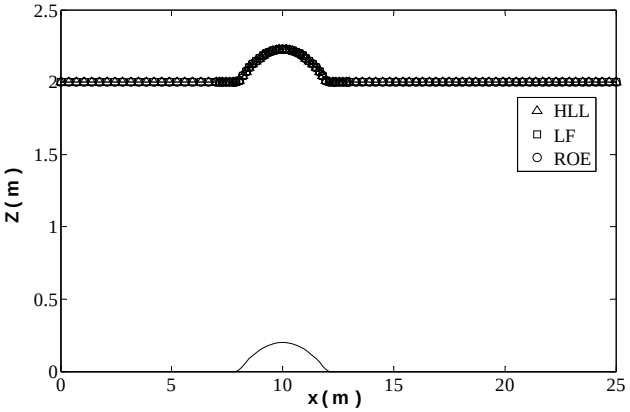

Fig. 13 Numerical solution of water depth for Test 4 with water depth slope limiter

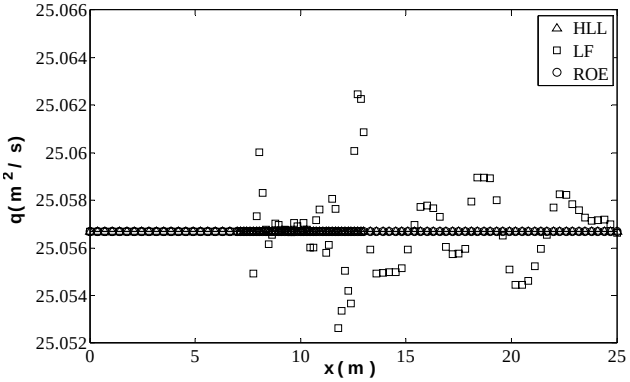

Fig. 14 Numerical solution of flow rate for Test 4 with water depth slope limiter

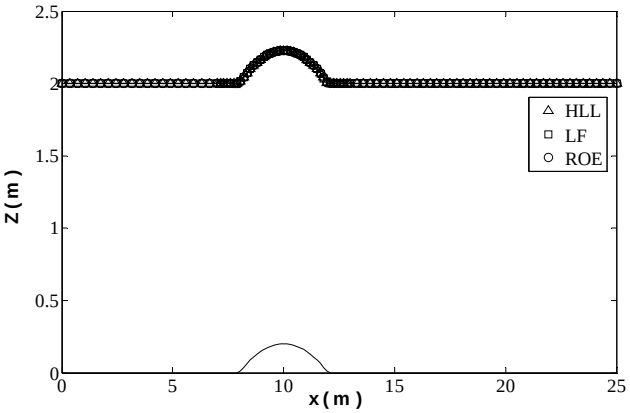

Fig. 15 Numerical solution of water depth for Test 4 with water surface slope limiter

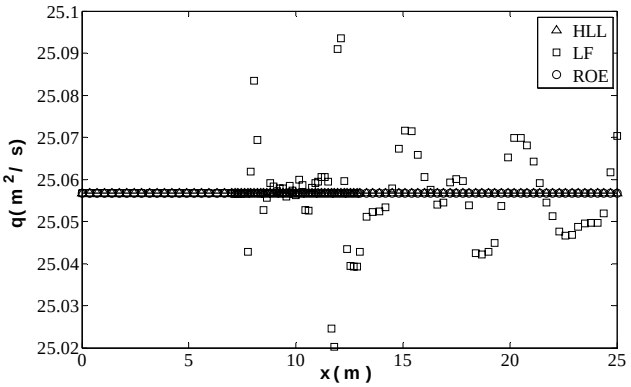

Fig. 16 Numerical solution of flow rate for Test 4 with water surface slope limiter

E. Test 5

In this test, a 1 m wide channel with bed topography given in Table I was used. There was no flow in or out of the domain and the initial water surface level was set to 16 *m*. The aim was to evaluate the performance of the numerical schemes in suppressing unphysical flow and flow depth oscillations.

TABLE I
BED ELEVATION VARIATION WITH DISTANCE

x (m)	z_b *(m)*	*x(m)*	z_b *(m)*
0	0	505	9
50	0	530	6
100	2.5	550	5.5
150	5	565	5.5
200	5	575	5
250	3	600	4
300	5	650	3
350	5	700	3
400	7.5	750	2.3
425	8	800	2
435	9	820	1.2
450	9	900	0.4
470	9	950	0
475	9.1	1000	0
500	9	1500	0

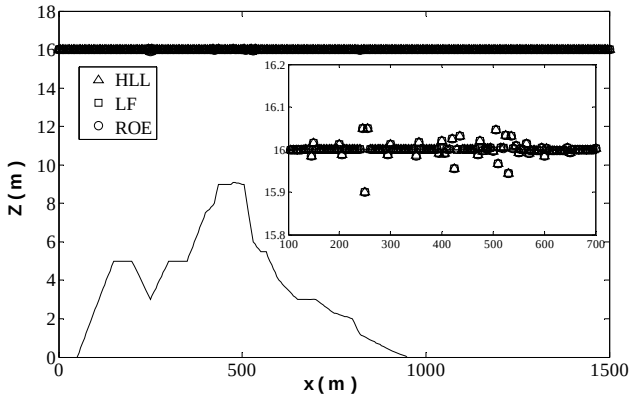

Fig. 17 Numerical solution of water depth for Test 5 with water depth slope limiter

The numerical results for water depth and flow rate are shown in Figs. 17 to 20. The results show the superiority of the slope limiter based on the water surface for preserving the initial condition of depth and zero flow rate. In case of the slope limiter based on the water depth, the Roe flux function provides the best result for maintaining the prescribed water depth and zero flow rate.

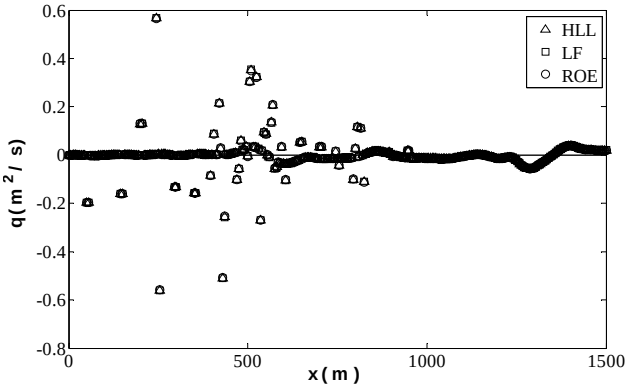

Fig. 18 Numerical solution of flow rate for Test 5 with water depth slope limiter

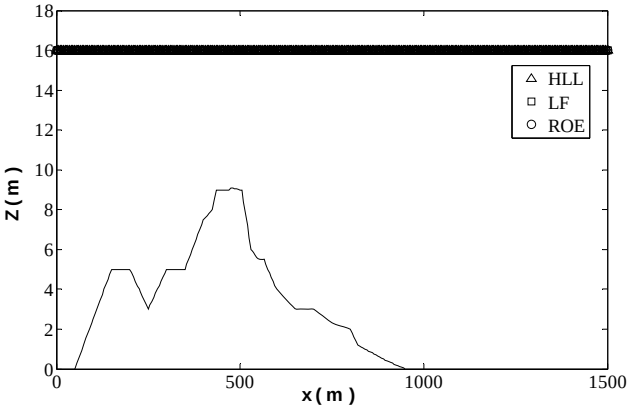

Fig. 19 Numerical solution of water depth for Test 5 with water surface slope limite

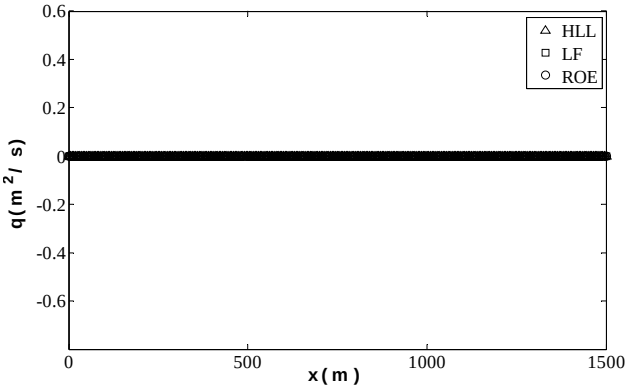

Fig. 20 Numerical solution of flow rate for Test 5 with water surface slope limite

F. Test 6

For the channel with irregular bed, as described in the previous test, the inflow rate was set to 10 m^2/s and the downstream water depth was set to 16 *m*. The flow regime throughout the channel is subcritical.

The simulation results for the water depth and flow rate are shown in Figs. 21 to 24. The water surface level is predicted accurately by slope limiters based on water surface and water depth with all three flux functions. However, the results for the flow rate exhibit oscillations in case of water depth based slope limiter with the LF flux providing the poorest results and the Roe flux the most accurate results. The water surface based slope limiter conserves the flow rate throughout the simulation domain with the Roe flux function providing the best results. A loss in flow rate is observed for the HLL and LF flux functions at the end of the channel.

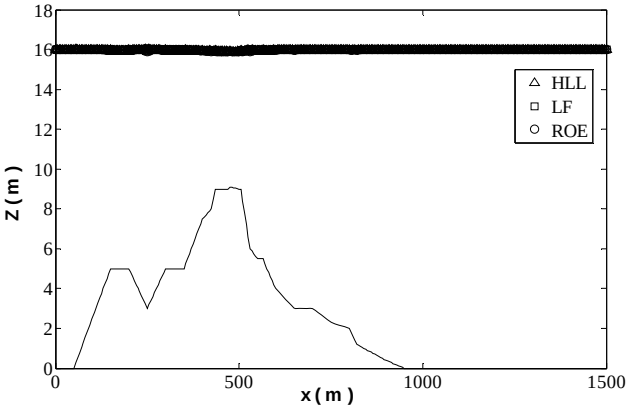

Fig. 21 Numerical solution of water depth for Test 6 with water depth slope limiter

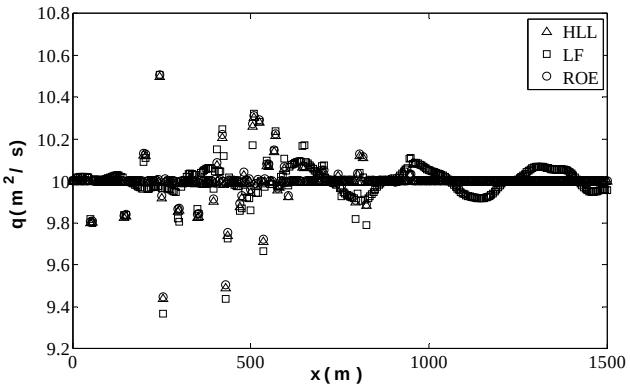

Fig. 22 Numerical solution of flow rate for Test 6 with water depth slope limiter

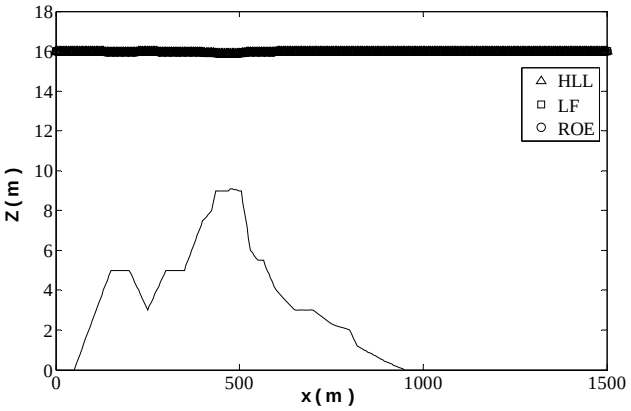

Fig. 23 Numerical solution of water depth for Test 6 with water surface slope limiter

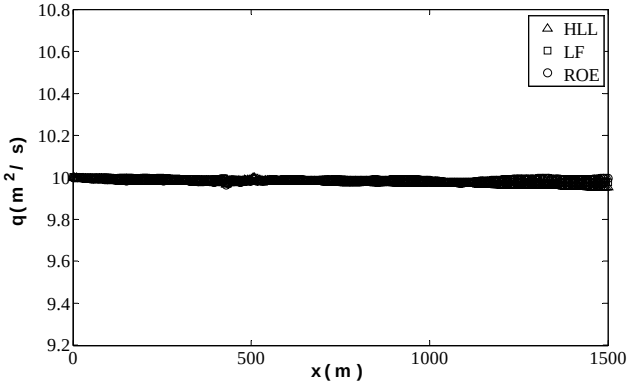

Fig. 24 Numerical solution of flow rate for Test 6 with water surface slope limiter

G. Test 7

With the irregular bed topography as described for Test 6, the flow rate at the inlet was set to 100 m^2/s and the depth at the downstream end was maintained at 16 *m*. In this test, the flow regime consists of both subcritical and supercritical flow with a hydraulic jump.

The numerical results, presented in Figs 25 to 28, show that while the water depth is predicted accurately by both slope limiter schemes, the flow rate is predicted more accurately by water surface based slope limiter. In addition, the Roe flux function provides better results for the flow rate when used with either slope limiter scheme.

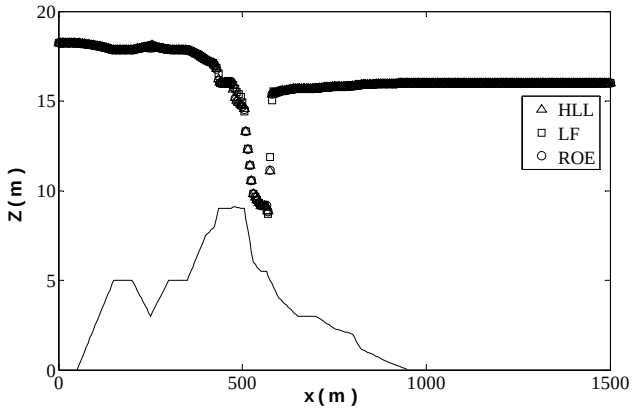

Fig. 25 Numerical solution of water depth for Test 7 with water depth slope limiter

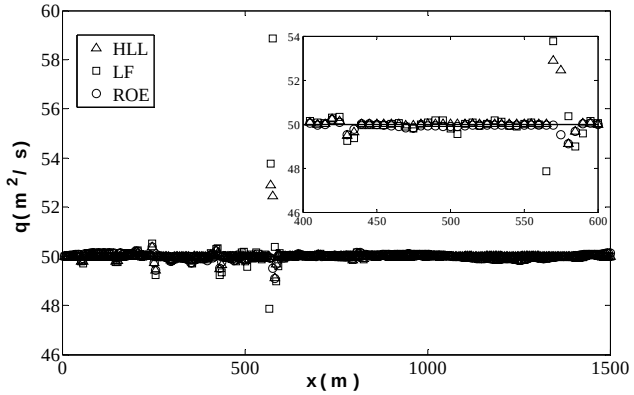

Fig. 26 Numerical solution of flow rate for Test 7 with water depth slope limiter

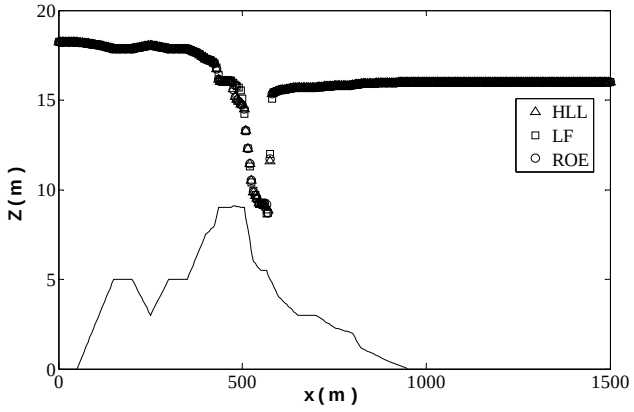

Fig. 27 Numerical solution of water depth for Test 7 with water surface slope limiter

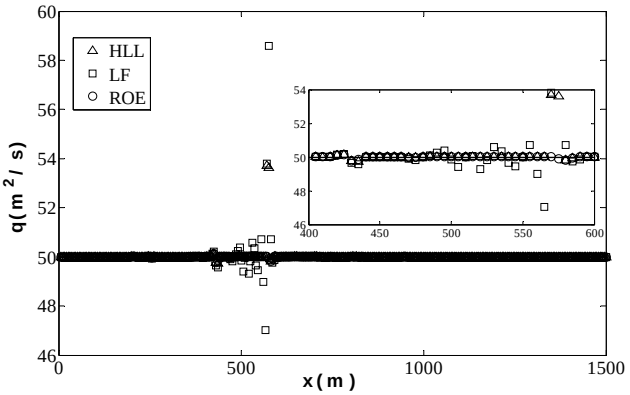

Fig. 28 Numerical solution of flow rate for Test 7 with water surface slope limiter

VII. Conclusion

The slope limiter scheme based on the water depth shows that even for the still water condition (Tests 1 and 5) the zero discharge is not preserved, with all three flux functions providing similar results. The results show that the non-physical bed slope generated flow increases as the bed becomes more irregular. In the case of water surface based slope limiter, the nonphysical flow is kept to minimal using all three flux functions, thus achieving better mass conservation. In the case of subcritical flow throughout the domain (Tests 2 and 6), the flow rate results based on the two slope limiter schemes follow the same trend as for still water case. However, the results for the flow rate show that overall the LF flux function performs the worst in conserving the flow rate while the Roe flux function has the best overall conservation property. In addition, water depth oscillations are observed with the use of water depth based slope limiter where there is abrupt bed slop change.

In the case where the flow transitions from subcritical to supercritical followed by a hydraulic jump, as in Tests 3 and 7, both slope limiter schemes provide similar albeit oscillatory results for the flow rate with LF flux function. For both slope limiter schemes, the Roe flux formulation conserves the flow rate most accurately. However, the use of water surface slope limiter with Roe flux provides the best solution. In the case of supercritical flow throughout the domain (Test 4), LF flux function is unable to conserve the initial flow rate.

In general, the water surface based slope limiter is better suited for open channel flows with irregular bed. The tests performed show that the Roe flux function has the best conservation property among the evaluated flux functions.

References

[1] J. S. Wang, H. G. Ni and Y. S. He, "Finite-difference TVD scheme for computation of dam-break problems," J. Hydr. Engng., vol. 126, no. 4, pp. 253-262, 2000.

[2] G. F. Lin, J. S. Lai and W. D. Guo, "Finite-volume component-wise TVD schemes for 2D shallow water equations," Adv. Water Resour., vol. 26, no. 8, pp. 861-873, 2003.

[3] T. J. R. Hughes, W. K. Liu and A. Brooks, "Finite element analysis of incompressible viscous flows by the penalty function formulation," J. Comput. Phys., vol. 30, no. 1, pp. 1-60, 1979.

[4] O. C. Zienkiewicz and P. Ortiz, "A split-characteristic based finite element model for the shallow equations," Int. J. Numer. Methods Fluids, vol. 20, no. 8-9, pp. 1061-1080, 1995.
[5] T. Arbogast and M. F. Wheeler, "A characteristics-mixed finite element method for advection-dominated transport problems," SIAM J. Numer. Anal., vol. 32, no. 2, pp. 404-424, 1995.
[6] W. H. Reed and T. Hill, "Triangular Mesh Method for the Neutron Transport Equation," Los Alamos Report, LA-UR-73-479, 1973.
[7] B. Cockburn and C. W. Shu, "TVB Runge-Kutta local projection discontinuous Galerkin finite element method for conservation laws II: General framework," Math. Comp., vol. 52, pp. 411-435, 1989.
[8] B. Cockburn, S. Y. Lin and C. W. Shu, "TVB Runge-Kutta local projection discontinuous Galerkin finite element method for conservation laws III: One dimensional systems," J. Comput. Phys, vol. 84, no. 1, pp. 90-113, 1989.
[9] B. Cockburn, S. Hou and C. W. Shu, "The Runge-Kutta local projection discontinuous Galerkin finite element method for conservation laws. IV: The multidimensional case," Math. Comp., vol. 54, pp. 545-581, 1990.
[10] B. Cockburn and C. W. Shu, "The Runge-Kutta discontinuous Galerkin finite element method for conservation laws V: Multidimensional systems," J. Comput. Phys., vol. 141, no. 2, pp. 199-224, 1998.
[11] B. Q. Li, "*Discontinuous Finite Elements in Fluid Dynamics and Heat Transfer*," Springer Verlag, 2006.
[12] D. Schwanenberg and J. Köngeter, "A discontinuous Galerkin method for the shallow water equations with source terms," Lecture Notes in Computational Science and Engineering, Springer, Berlin, vol. 11, pp. 419-424, 2000.
[13] D. Schwanenberg and M. Harms, "Discontinuous Galerkin finite-element method for transcritical two-dimensional shallow water flows," J. Hydr. Engng., vol. 130, no. 5, pp. 412-421, 2004.
[14] V. Aizinger and C. Dawson, "A discontinuous Galerkin method for two-dimensional flow and transport in shallow water," Adv. Water Resour., vol. 25, no. 1, pp. 67-84, 2002.
[15] C. Dawson and V. Aizinger, "A discontinuous Galerkin method for three-dimensional shallow water equations," J. Sci. Comput., vol. 22, no. 1, pp. 245-267, 2005.
[16] E. J. Kubatko, J. J. Westerink and C. Dawson, "hp discontinuous Galerkin methods for advection dominated problems in shallow water flow," Comput. Methods Appl. Mech. Eng., vol. 196, no, 1-3, pp. 437-451, 2006.
[17] A. Harten, P. D. Lax and B. van Leer, "On upstream differencing and Godunov-type schemes for hyperbolic conservation laws," SIAM Rev., vol. 25, no. 1, pp. 35-61, 1983.
[18] P. Roe, "Approximate Riemann solvers, parameter vectors, and difference schemes," J. Comput. Phys., vol. 43, no. 2, pp. 357-372, 1981.
[19] P. Tassi, O. Bokhove and C. Vionnet, "Space discontinuous Galerkin method for shallow water flows—kinetic and HLLC flux, and potential vorticity generation," Adv. Water Resour., vol. 30, no. 4, pp. 998-1015, 2007.
[20] S. Gottlieb and C. W. Shu, "Total variation diminishing Runge-Kutta schemes," Math. Comp., vol. 67, 73-85, 1998.
[21] J. G. Zhou, D. M. Causon, C. G. Mingham and D. M. Ingram, "The surface gradient method for the treatment of source terms in the shallow-water equations," J. Comput. Phys., vol. 168, no. 1, pp. 1-25, 2001.
[22] X. Ying, A. A. Khan and S. S. Y. Wang, "Upwind conservative scheme for the Saint Venant equations," J. Hydr. Engng., vol. 130, no. 4, pp. 977-987, 2004.
[23] M. Catella, E. Paris and L. Solari, "Conservative scheme for numerical modeling of flow in natural geometry," J. Hydr. Engng., vol. 134, no. 6, pp. 736-748, 2008.
[24] B. Cockburn, "Discontinuous Galerkin Methods for Convection Dominated Problems," Lecture Notes in Computational Science and Engineering, Springer, Berlin, vol. 9, pp. 69-224, 2001.